Solid State Ionics 341 (2019) 115023

Contents lists available at ScienceDirect

Solid State Ionics

journal homepage: www.elsevier.com/locate/ssi

The copper argyrodites $Cu_{7-n}PS_{6-n}Br_n$: Crystal growth, structures and ionic conductivity

A.I. Pogodin*, M.J. Filep, T.O. Malakhovska, M.Yu. Sabov, V.I. Sidey, O.P. Kokhan, I.P. Studenyak

Uzhhorod National University, Pidgirna Street 46, Uzhhorod 88000, Ukraine

ARTICLE INFO

Keywords:
Argyrodites
Crystal growth
Structure
Ionic conductivity
Activation energy
Compositional dependence

ABSTRACT

Single crystals of the copper-containing $Cu_{7-n}PS_{6-n}Br_n$ ($0 \le n \le 1$) argyrodites have been grown by direct solidification using the Bridgman–Stockbarger technique. All compounds have been structurally characterized using the X-ray powder diffraction technique. Compositional dependencies of electrical conductivity and activation energy were studied. Two simple structural indicators have been proposed in order to predict the ionic conductivity in argyrodites under investigations. Interrelation between structure and mechanism of ionic conductivity was discussed.

1. Introduction

The crystalline $Cu_{7-n}PS_{6-n}X_n$ (X = Cl, Br, I; $0 \le n \le 1$) argyrodites belong to a large family of the tetrahedrally close-packed structures [1,2]. They are characterized by high concentration of disordered vacancies for the Cu^+ cations and reveal promising superionic, ferroelastic and nonlinear optical properties, the ionic conductivity being attributed to the order-disorder phenomena in the Cu^+ sublattice [1,2]. This paper is a continuation of the systematic investigations of Cu_6PS_5X argyrodites, which have been carried out over the last few decades [3–10].

It should be noted, however, that all $Cu_{7-n}PS_{6-n}X_n$ single crystals investigated earlier have been grown by using the chemical vapor transport (CVT) technique [11] and were rather small in size (typically < 5 mm in all dimensions [4,5]). Our attempts to obtain larger $Cu_{7-n}PS_{6-n}X_n$ crystals by CVT were unsuccessful; so, in order to enhance the applicability of the above described copper argyrodites, we decided to develop an alternative growth procedure suitable for obtaining the larger $Cu_{7-n}PS_{6-n}X_n$ single-crystalline samples.

In the last decade, lithium-containing Li_6PS_5X (X = Cl, Br, I) argyrodite superionic conductors have been actively studied as promising materials for all-solid-state batteries [12–15]. Thus, the all-solid-state cell using the Li_6PS_5Br fine powder with a high conductivity of 1 mS/cm demonstrated a reversible capacity of 150 mA × h/g [15]. Even though the lithium-containing argyrodites are very promising, the studies of new copper-containing superionic argyrodites is currently of great importance due to the possibilities of their preparation in a simple and economical way.

Thus, this work is aimed to present the new method developed to obtain the stoichiometric $Cu_{7-n}PS_{6-n}Br_n$ ($0 \le n \le 1$) single crystals. Additionally, all they have been structurally characterized using the powder X-ray diffraction (XRD) technique, and simple structural indicators have been proposed in order to predict the ionic conductivity of the argyrodites under investigation.

2. Experimental

2.1. Synthesis and crystal growth

Based on the phase diagram, constructed earlier for the quasiternary Cu_2S–CuBr–"P_2S_5" system in Ref. [16], the virtually optimum conditions have been established for obtaining the single crystals of the stoichiometric ternary (Cu_7PS_6) and quaternary (Cu_6PS_5Br) compounds as well as $Cu_{7-n}PS_{6-n}Br_n$ ($0 < n < 1$) solid solutions on their base. The formation of solid solutions occurs as a result of the heterovalent substitution in the argyrodite structure with charge compensation according to the scheme $Cu^+ + S^{2-} \leftrightarrow Br^- + \square$. As the above mentioned stoichiometric compounds melt congruently, and because of the quite

* Corresponding author.
E-mail address: artempogodin88@gmail.com (A.I. Pogodin).

https://doi.org/10.1016/j.ssi.2019.115023
Received 14 November 2018; Received in revised form 5 July 2019; Accepted 7 July 2019

Table 1
Parameters of the direct solidification growing processes for $Cu_{7-n}PS_{6-n}Br_n$ single crystals.

Composition	Highest temperature (K)	Annealing temperature (K)	Temperature gradient in crystallization zone (K/mm)	Growing rate (mm/day)
Cu_7PS_6	1380	973	3–4	10–12
$Cu_{6.9}PS_{5.9}Br_{0.1}$	1375	923	3–4	10–12
$Cu_{6.8}PS_{5.8}Br_{0.2}$	1370	923	3–4	10–12
$Cu_{6.75}PS_{5.75}Br_{0.25}$	1365	923	3–4	10–12
$Cu_{6.5}PS_{5.5}Br_{0.5}$	1355	923	3–4	10–12
$Cu_{6.25}PS_{5.25}Br_{0.75}$	1345	923	3–4	10–12
$Cu_{6.1}PS_{5.1}Br_{0.9}$	1335	923	3–4	10–12
Cu_6PS_5Br	1350	973	3–4	10–12

subtle differences between the melting and solidification temperatures of the considered solid solutions, their single crystals could successfully be grown by direct solidification using the Bridgman–Stockbarger technique, in evacuated silica ampoules with the specially shaped tips.

The main peculiarity of the method used to obtain single crystals of the Cu_7PS_6 and Cu_6PS_5Br compounds and their solid solutions is the fact that the ampoules were filled with the starting components (Cu, P, S, CuBr) rather than with the previously synthesized single-phase mixture. The initial binary CuBr was obtained from the initial Cu and Br_2, taken in stoichiometric ratios, by means of two-temperature synthesis in a vacuum quarz ampoule and further purified by vacuum distillation.

This method makes it possible to synthesize the copper-containing chalcogenides with no deviation from stoichiometry and/or with the specially preset compositions. Additionally, this method prevents undesired deviations from stoichiometry (and also from the preset compositions), caused by unavoidable losses of materials at the interim stages of manipulations with mixtures. All the chemicals used in this work were of a purity of 99.999 wt% or better.

The optimum conditions of the direct solidification growing processes used to obtain the single crystals of $Cu_{7-n}PS_{6-n}Br_n$ ($0 \le n \le 1$) argyrodites are presented in Table 1. The melts were held at the highest temperature for 24 h. After the crystals have been grown, they were annealed (at the properly selected annealing temperature quoted in Table 1) for 3 days in order to remove internal strains. Using the above method of synthesis and the conditions listed in Table 1, the single crystals of $Cu_{7-n}PS_{6-n}Br_n$ ($0 \le n \le 1$) argyrodites with the lengths of 30–40 mm and diameters of 10–15 mm have been grown. Some examples of the grown crystals are presented in Fig. 1.

2.2. Crystal structure determination

The crystal structures of the $Cu_{7-n}PS_{6-n}Br_n$($0 \le n \le 1$) argyrodites were studied using XRD technique. XRD data were collected with a conventional Bragg–Brentano diffractometer DRON–4-07 in the step-scan mode (Ni-filtered CuKα radiation, $10^\circ \le 2\theta \le 80^\circ$, step size 0.02°, counting time 10 s per step, room temperature).

Automatic indexing of XRD patterns, space-group checking/assignment, the Rietveld refinement [17,18] procedures and difference Fourier syntheses (to complete the structure models) have been performed using the program EXPO-2014 (with the default presets) by Altomare and co-workers [19]. In the Rietveld refinement, the main criterion for quality of the structural model obtained was the R_F-factor [18] which, unlike the "profile" R-factors, is not affected by the background level of an XRD pattern [20].

All the Rietveld refinement calculations (Fig. 2) were quite stable and straightforward, so the human control of the refinement strategy was typically limited to (i) fixing the isotropic atomic displacement parameters B_{iso} to some physically plausible values, (ii) keeping (during the earlier refinement circles) the P-S interatomic distances of the coordination [PS_4] tetrahedra at the typical values [21], (iii) turning on/off (when required) the refinement of the site occupancy factors (SOF). During refinement, no restrictions were imposed on occupancy of the S/Br positions, nor on the chemical composition. These parameters were determined during the refinement.

The results of the crystal structure determination for $Cu_{7-n}PS_{6-n}Br_n$($0 \le n \le 1$) argyrodites are summarized in Table 2. The nominal and experimentally determined (based on the Rietveld refinement) compositions of $Cu_{7-n}PS_{6-n}Br_n$($0 \le n \le 1$) argyrodites are given in Table 3, along with the corresponding space groups and lattice parameters.

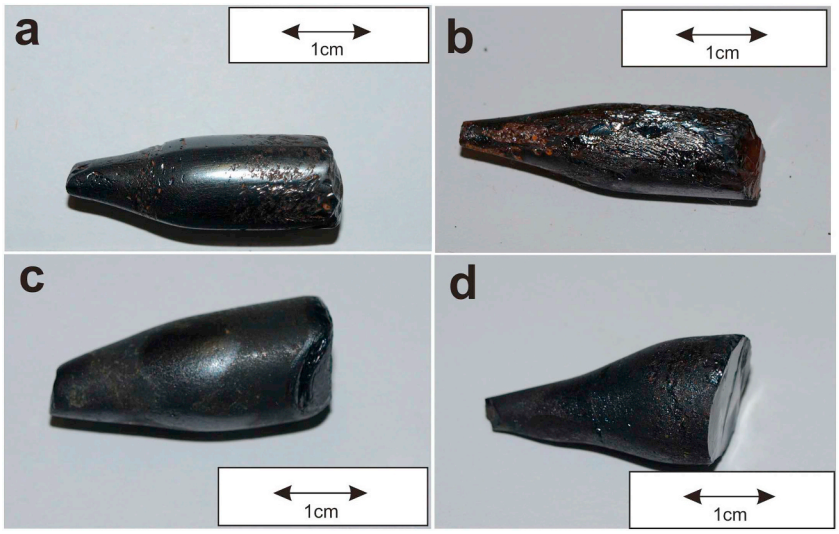

Fig. 1. Images of $Cu_{7-n}PS_{6-n}Br_n$ single crystals: Cu_7PS_6 (a), Cu_6PS_5Br (b), $Cu_{6.25}PS_{5.25}Br_{0.75}$ (c), and $Cu_{6.75}PS_{5.75}Br_{0.25}$ (d).

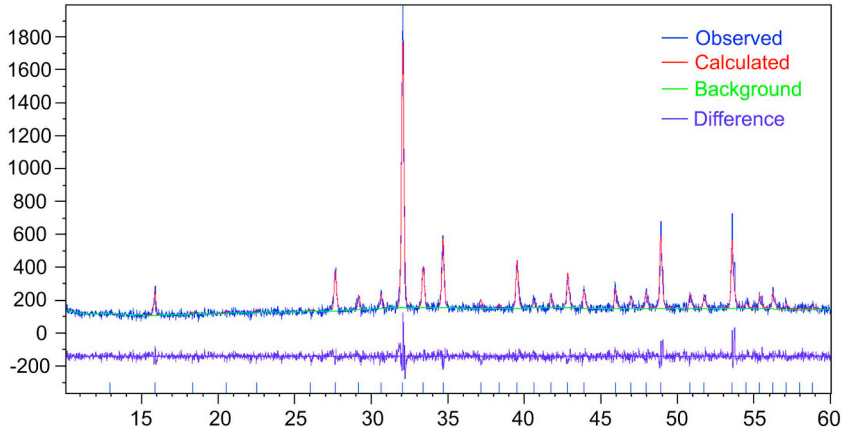

Fig. 2. XRD pattern and results of refinement for $Cu_{6.85}PS_{5.85}Br_{0.15}$ solid solution.

Table 2
Parameters of crystal structure models for $Cu_{7-n}PS_{6-n}Br_n$ compounds (positions, coordinates (x, y, z), isotropic atomic displacement parameters B_{iso}, and site occupancy factors (SOF); fixed values are marked with an asterisk *).

Atom	Position	x	y	z	B_{iso} (Å^2)	SOF
Cu_7PS_6: $P2_13$, a = 9.668 Å, Z = 4; R_F = 4.34%; R_{wp} = 7.06%						
S1	4a	0.4707	0.4707	0.4707	5.484	0.964
S2	12b	0.1361	−0.1078	0.1310	0.500*	1.000
S3	4a	0.1408	0.3592	0.6408	0.500*	1.000
S4	4a	0.2376	0.2376	0.2376	0.500*	1.000
P1	4a	0.2643	0.2357	0.7643	0.500*	1.000
Cu1	12b	0.0637	0.2350	0.4263	2.006	0.943
Cu2	12b	−0.0275	−0.0119	0.2698	0.500*	0.732
Cu3	12b	0.0722	0.0787	0.2755	0.261	0.347
Cu4	4a	0.3659	0.3659	0.3659	5.501	0.927
$Cu_{6.9}PS_{5.9}Br_{0.1}$: $P2_13$, a = 9.675 Å, Z = 4; R_F = 3.29%; R_{wp} = 3.29%						
Br	4a	0.2360	0.2360	0.2360	0.095	0.094
S1	4a	0.4744	0.4744	0.4744	0.229	0.946
S2	12b	0.1396	−0.1162	0.1315	0.500*	1.000
S3	4a	0.1475	0.3525	0.6475	0.500*	1.000
S4	4a	0.2418	0.2418	0.2418	0.500*	0.906
P1	4a	0.2603	0.2397	0.7603	0.500*	1.000
Cu1	12b	0.0682	0.2345	0.4242	3.075	0.971
C1u2	12b	−0.0225	−0.0143	0.2765	0.500*	0.710
Cu3	12b	0.0404	0.0942	0.2370	0.536	0.353
Cu4	4a	0.3693	0.3693	0.3693	2.845	0.803
$Cu_{6.85}PS_{5.85}Br_{0.15}$: $P2_13$, a = 9.673 Å, Z = 4; R_F = 4.75%; R_{wp} = 7.62%						
Br	4a	0.2326	0.2326	0.2326	0.500*	0.144
S1	4a	0.4773	0.4773	0.4773	2.835	1.000
S2	12b	0.1350	−0.1190	0.1291	0.500*	1.000
S3	4a	0.1444	0.3556	0.6444	0.500*	1.000
S4	4a	0.2437	0.2437	0.2437	0.500*	0.856
P1	4a	0.2551	0.2449	0.7551	0.500*	1.000
Cu1	12b	0.0731	0.2334	0.4264	3.264	0.943
Cu2	12b	−0.205	−0.0181	0.2749	0.638	0.753
Cu3	12b	0.0405	0.0879	0.2351	0.500*	0.339
Cu4	4a	0.3711	0.3711	0.3711	2.047	0.777
$Cu_{6.8}PS_{5.8}Br_{0.2}$: $P2_13$, a = 9.676 Å, Z = 4; R_F = 6.02%; R_{wp} = 5.84%						
Br	4a	0.2417	0.2417	0.2417	0.052	0.227
S1	4a	0.4935	0.4935	0.4934	0.583	1.000
S2	12b	0.1383	−0.1270	0.1372	0.500*	1.000
S3	4a	0.1427	0.3573	0.6427	0.500*	1.000
S4	4a	0.2407	0.2407	0.2407	0.500*	0.798
P1	4a	0.2549	0.2451	0.7549	0.500*	1.000
Cu1	12b	0.0782	0.2306	0.4246	3.376	0.924
Cu2	12b	−0.0113	−0.0111	0.2783	0.500*	0.781
Cu3	12b	0.0719	0.0856	0.2480	2.223	0.320
Cu4	4a	0.3651	0.3651	0.3651	3.298	0.697
$Cu_{6.5}PS_{5.5}Br_{0.5}$: $P2_13$, a = 9.685 Å, Z = 4; R_F = 9.43%; R_{wp} = 7.73%						
Br	4a	0.2581	0.2581	0.2581	0.144	0.501
S1	4a	0.5032	0.5032	0.5032	0.523	1.000
S2	12b	0.1282	−0.1224	0.1299	0.500*	1.000

(*continued on next page*)

Table 2 (*continued*)

Atom	Position	*x*	*y*	*z*	B_{iso} (Å^2)	SOF
S3	4a	0.1316	0.3684	0.6316	0.500*	1.000
S4	4a	0.2308	0.2308	0.2308	0.500*	0.500
P1	4a	0.2539	0.2461	0.7539	0.500*	1.000
Cu1	12b	0.0645	0.2318	0.4462	5.037	0.845
Cu2	12b	−0.0224	−0.0274	0.2754	0.041	0.709
Cu3	12b	0.0548	0.0754	0.2522	0.309	0.389
Cu4	4a	0.3806	0.3806	0.3806	7.155	0.663
$Cu_{6.25}PS_{5.25}Br_{0.75}$: *F-43 m*, *a* = 9.694 Å, Z = 4; R_F = 9.71%; R_{wp} = 5.27%						
Br1	4a	0.5000	0.5000	0.0000	2.083	0.720
S1	16e	0.3848	0.1152	−0.1152	0.500*	1.000
S2	4c	0.2500	0.2500	0.2500	0.217	1.000
S3	4a	0.5000	0.5000	0.0000	0.504	0.280
P1	4b	0.5000	0.0000	0.0000	0.810	1.000
Cu1	24 g	0.2500	0.2500	0.0212	0.194	0.469
Cu2	48 h	0.3423	0.3423	0.0310	2.675	0.286
$Cu_{6.1}PS_{5.1}Br_{0.9}$: *F-43 m*, *a* = 9.698 Å, Z = 4; R_F = 6.04%; R_{wp} = 5.10%						
Br1	4a	0.5000	0.5000	0.0000	3.865	0.889
S1	16e	0.3862	0.1138	−0.1138	0.500*	1.000
S2	4c	0.2500	0.2500	0.2500	0.431	1.000
S3	4a	0.5000	0.5000	0.0000	0.601	0.111
P1	4b	0.5000	0.0000	0.0000	0.872	1.000
Cu1	24 g	0.2500	0.2500	0.0242	0.013	0.496
Cu2	48 h	0.3464	0.3464	0.0298	1.915	0.259
Cu_6PS_5Br: *F-43 m*, *a* = 9.701 Å, Z = 4; R_F = 9.54%; R_{wp} = 8.86%						
Br1	4a	0.5000	0.5000	0.0000	3.453	1.000
S1	16e	0.3833	0.1167	−0.1167	0.500*	1.000
S2	4c	0.2500	0.2500	0.2500	0.512	1.000
P1	4b	0.5000	0.0000	0.0000	0.862	1.000
Cu1	24 g	0.2500	0.2500	0.0235	0.244	0.488
Cu2	48 h	0.3461	0.3461	0.0296	1.539	0.255

Table 3
Nominal and refined (from the XRD experiments) compositions, space groups and lattice parameters *a* of $Cu_{7-n}PS_{6-n}Br_n$ compounds.

Nominal composition	Composition by XRD	Space group	Lattice parameter *a* (Å)
Cu_7PS_6	$Cu_{6.99}PS_{5.96}$	*P2$_1$3*	9.668
$Cu_{6.9}PS_{5.9}Br_{0.1}$	$Cu_{6.91}PS_{5.89}Br_{0.09}$	*P2$_1$3*	9.675
$Cu_{6.85}PS_{5.85}Br_{0.15}$	$Cu_{6.88}PS_{5.86}Br_{0.14}$	*P2$_1$3*	9.673
$Cu_{6.8}PS_{5.8}Br_{0.2}$	$Cu_{6.77}PS_{5.79}Br_{0.21}$	*P2$_1$3*	9.676
$Cu_{6.5}PS_{5.5}Br_{0.5}$	$Cu_{6.49}PS_{5.5}Br_{0.5}$	*P2$_1$3*	9.685
$Cu_{6.25}PS_{5.25}Br_{0.75}$	$Cu_{6.25}PS_{5.28}Br_{0.72}$	*F-43m*	9.694
$Cu_{6.1}PS_{5.1}Br_{0.9}$	$Cu_{6.08}PS_{5.11}Br_{0.89}$	*F-43m*	9.698
Cu_6PS_5Br	$Cu_{5.99}PS_5Br$	*F-43m*	9.701

2.3. Measurement of ionic conductivity

The values of the ionic conductivity of the samples were measured by the AC impedance method using an AC bridge P568 over the frequency range from 20 Hz to 90 kHz and the temperature interval from 295 to 353 K [22]. The temperature was controlled with an UTU–4 thermostat. 1 M $Cu(NO_3)_2$ solution was used as the contacts, in accordance with the scheme presented in Fig. 3. The general equivalent circuit used for explanation of the processes on the crystal-electrolyte interface is shown on Fig. 3, where W_B is the element of the resulting diffusion, R and C are the volume resistance and capacity, respectively, while R_d and C_d are the resistance and capacity of the diffusion layer, respectively.

Some examples of the Nyquist plots obtained in the impedance measurements for the investigated samples are presented in Fig. 4. The temperature dependencies of the ionic conductivity, the Arrhenius plots and calculated activation energy of the crystals in the Cu_7PS_6–Cu_6PS_5Br quasibinary system are shown in Fig. 5.

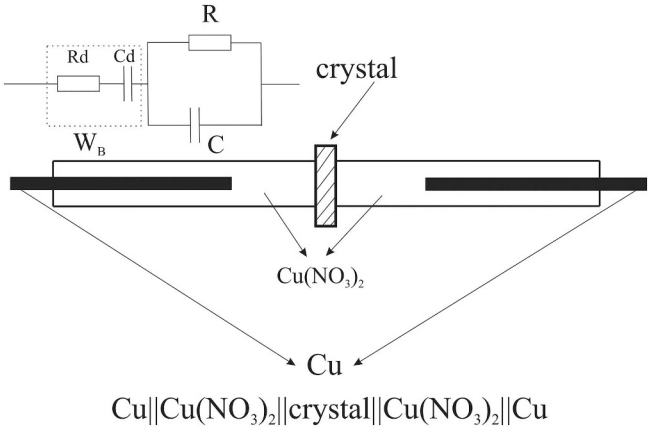

Fig. 3. Scheme of the cell for the impedance measurements and equivalent circuit used for the explanation of the processes on the crystal-electrolyte interface of the $Cu_{7-n}PS_{6-n}Br_n$ crystals.

3. Results and discussion

Cu_7PS_6 compound crystallizes in the space group *P2$_1$3* with the lattice parameter *a* = 9.668 Å, the formula unit per cell *Z* = 4.

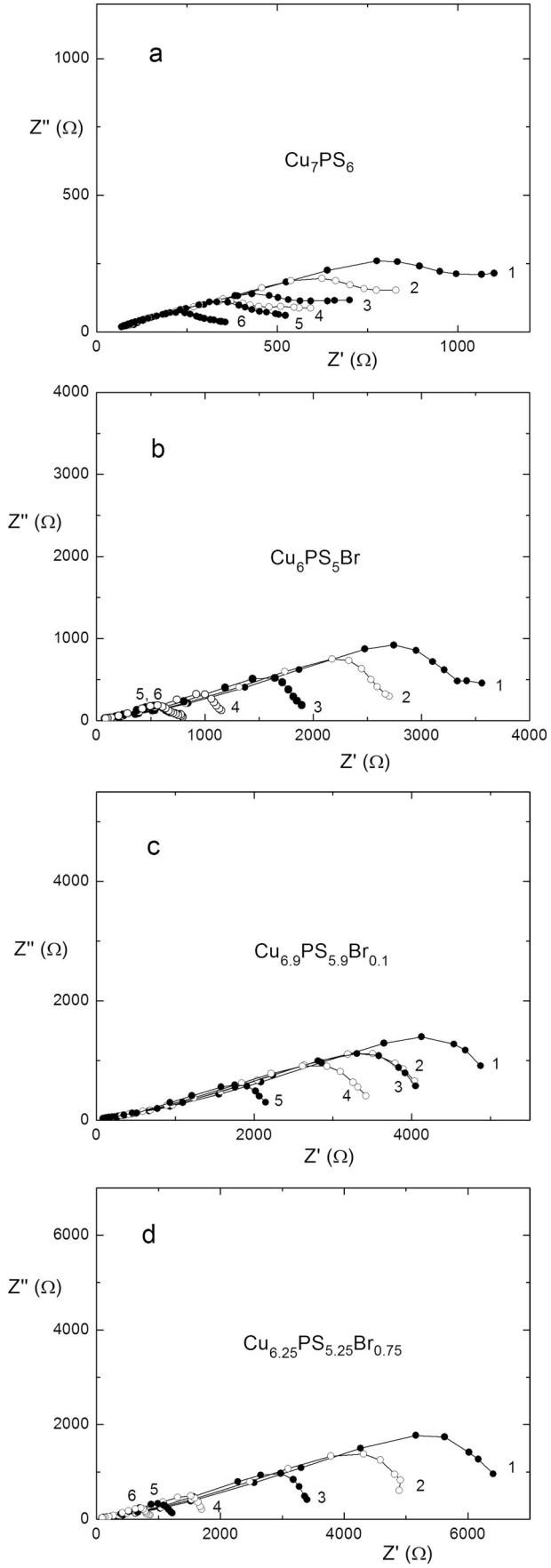

Fig. 4. Nyquist plots for Cu_7PS_6 (a), Cu_6PS_5Br (b), $Cu_{6.9}PS_{5.9}Br_{0.1}$ (c), and $Cu_{6.25}PS_{5.25}Br_{0.75}$ (d) single crystals at various temperatures: 303 K (1), 313 K (2), 323 K (3), 333 K (4), 343 K (5) and 353 K (6).

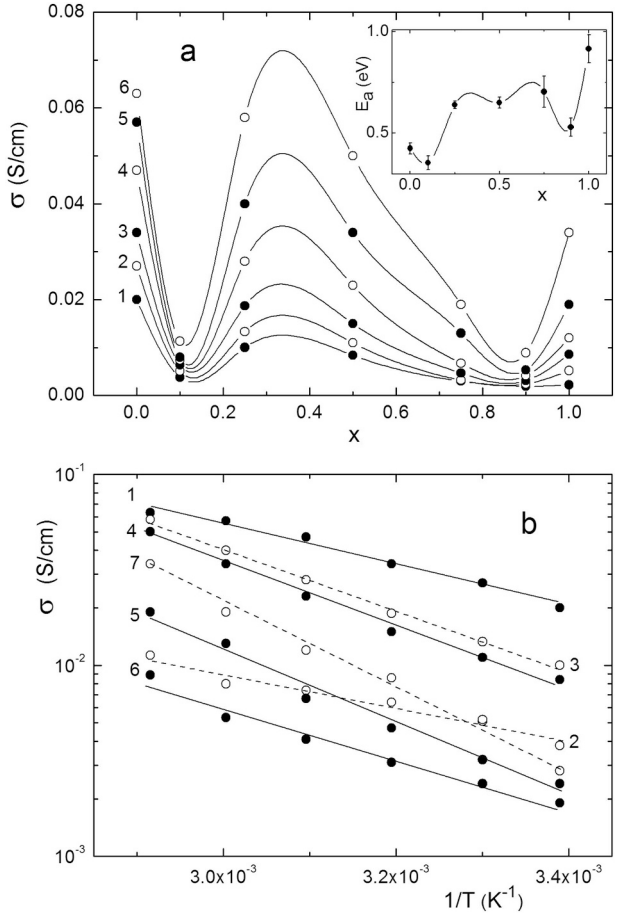

Fig. 5. (a) Compositional dependencies of ionic conductivity for $Cu_{7-n}PS_{6-n}Br_n$ crystals at various temperatures: 295 K (1), 303 K (2), 313 K (3), 323 K (4), 333 K (5) and 343 K (6). The inset shows the compositional dependence of activation energy for $Cu_{7-n}PS_{6-n}Br_n$ crystals. (b) Arrhenius plots for $Cu_{7-n}PS_{6-n}Br_n$ crystals: Cu_7PS_6 (1), $Cu_{6.9}PS_{5.9}Br_{0.1}$ (2), $Cu_{6.75}PS_{5.75}Br_{0.25}$ (3), $Cu_{6.5}PS_{5.5}Br_{0.5}$ (4), $Cu_{6.25}PS_{5.25}Br_{0.75}$ (5), $Cu_{6.1}PS_{5.1}Br_{0.9}$ (6), and Cu_6PS_5Br (7).

Structure of Cu_7PS_6 is formed by a rigid framework built of the $[PS_4]$ and $[SS_4]$ tetrahedra (Fig. 6); the copper atoms being placed on the faces/edges and in the interstices of the latter tetrahedra.

The anion sublattice of Cu_7PS_6 structure can also be viewed as a framework built of interpenetrating centered (by the sulfur atoms S2 and S3) icosahedra $[SS_{12}]$ (Fig. 7) formed by the $[PS_4]$ and $[\varnothing S_4]$ coordination tetrahedra ($\varnothing$ depicts the vacancy of the central atom).

The copper atoms in Cu_7PS_6 structure are either 4-coordinated (Cu1, Cu2 and Cu3) or 2-coordinated (Cu4) by sulfur atoms. Fig. 7(c, d) illustrates different types of coordination of the copper atoms in Cu_7PS_6 structure.

Cu_6PS_5Br compound crystallizes in the space group *F-43 m* with the lattice parameter $a = 9.701$ Å, the formula unit per cell $Z = 4$. Obviously, the lattice parameter of Cu_6PS_5Br crystal grown by the method of directed crystallization from the melt differs from that of the data known in the literature [1,2]. This may be due to the more defective and intense structure of Cu_6PS_5Br, which is often observed for single crystals grown by "crucible" methods, in contrast to the samples obtained by CVT method, for which the growth ampoule does not limit the growth of the crystal. One can distinguish the $[PS_4]$ and $[SBr_4]$ tetrahedra of Cu_6PS_5Br structure, with the copper atoms placed on the faces/edges and in the interstices of the latter tetrahedra (Fig. 8). The anion sublattice of Cu_6PS_5Br structure can be viewed as interpenetrating icosahedra $[SS_9Br_3]$ (centered by the S1 atom) built of the $[PS_4]$, $[\varnothing S_4]$ and $[\varnothing S_3Br]$ coordination tetrahedra (Fig. 8c). Different

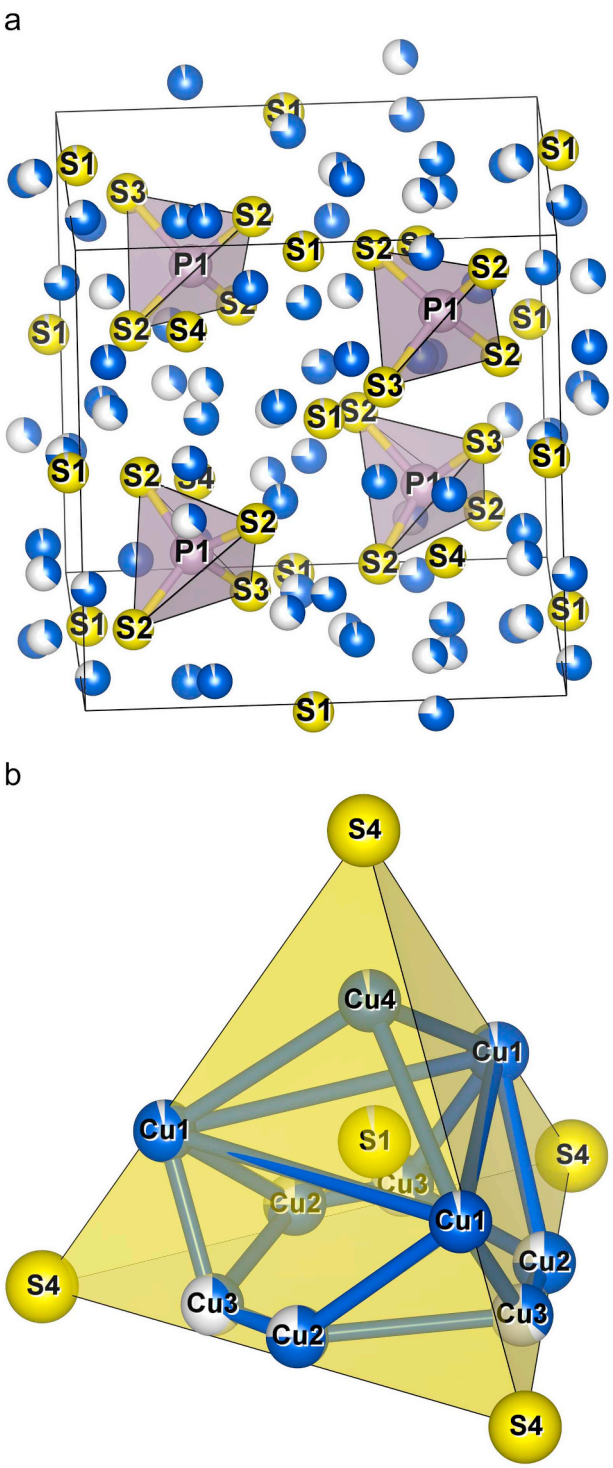

Fig. 6. Coordination tetrahedra [PS_4] (a) and [SS_4] (b) in the structure of Cu_7PS_6 (the bicolor spheres illustrate the atoms with partial SOF: the higher the occupancy the smaller fraction of the white color of the sphere).

coordination types of the symmetrically distinct copper atoms in the structure of Cu_6PS_5Br compound can be illustrated using the double tetrahedra [S_3Br_2] (Fig. 8d) analogous to those shown in Fig. 7(c, d). Thus, while the Cu1 atoms are surrounded by 3 sulfur atoms, the Cu2 atoms are tetrahedrally coordinated by 3 sulfur atoms and one Br atom.

As seen from Table 2 and Table 3, $Cu_{7-n}PS_{6-n}Br_n$ solid solutions exist in quite wide concentration ranges and have both *F-43 m* and *P2₁3* symmetry. During the refinement of the crystalline structures of solid solutions, we tried all variants of the heterovalent substitution $S^{2-} \leftrightarrow Br^-$, and based on the lowest values of *R* factors, the substitution position was established. Structurally, the formation of the solid solutions $Cu_{7-n}PS_{6-n}Br_n$ based on Cu_7PS_6 (*P2₁3*; $0 \le n \le 0.5$) can be viewed as a gradual replacement of the S4 atom (position 4a) with the Br atom, accompanied (i) with the changes in the SOF values of the copper atoms (to achieve the ionic charge balance) and (ii) with the changes in the atomic coordinates (to incorporate larger Br atoms into the structure). Similarly, the formation of the solid solutions based on Cu_6PS_5Br (*F-43 m*; $0.6 \le n \le 1$) can be viewed as a gradual replacement of the Br atom (position 4a) with the additional S3 atom, accompanied with the structural changes (to adapt the structure to a new charge balance and new spatial constraints) [23].

Analysis of the structural peculiarities of $Cu_{7-n}PS_{6-n}Br_n$ ($0 \le n \le 1$) argyrodites has revealed two simple indicators demonstrating the inverse correlations with the ionic conductivity of the crystals in the Cu_7PS_6–Cu_6PS_5Br system (Fig. 5). Thus, in accordance with the earlier findings [8], the ionic conductivity of the copper argyrodites are primarily defined by the migration of Cu^+ ions between the sites that (i) have the rather small SOF values, (ii) are reasonably close to each other, and (iii) have the twofold and threefold (nearly threefold) coordination by anion ligands. Taking these findings into account, one can conclude that the ionic conductivity observed for the samples investigated in this paper (Fig. 5) is defined by the migration of Cu2 and Cu3 atoms for Cu_7PS_6-based solid solutions and by the migration of Cu1 and Cu2 atoms for Cu_6PS_5Br-based solid solutions. In this respect, the sum of the SOF values (ΣSOF) of the positions of the above mentioned migrating Cu atoms and the longest symmetrically independent distance between these atoms $d(Cu\text{-}Cu)_{max}$ were expected to be valuable indicators for predicting the ionic conductivity of $Cu_{7-n}PS_{6-n}Br_n$ argyrodites.

Comparison of $d(Cu\text{-}Cu)_{max}$ (Fig. 9, curve 1) and ΣSOF (Fig. 9, curve 2) values with the ionic conductivity observed for the same $Cu_{7-n}PS_{6-n}Br_n$ argyrodites (Fig. 5) has clearly shown their strong inverse correlation. Hence, $d(Cu\text{-}Cu)_{max}$ and ΣSOF values could be recommended for use in further investigations of the copper argyrodites as tentative indicators/descriptors suitable for predicting the ionic conductivity from structural data.

4. Conclusions

The method suitable for growing large single crystal of $Cu_{7-n}PS_{6-n}Br_n$ ($0 \le n \le 1$) argyrodites by direct solidification has been developed, and the single-crystalline samples have been obtained over the whole concentration range from Cu_7PS_6 to Cu_6PS_5Br. Using the XRD technique $Cu_{7-n}PS_{6-n}Br_n$ ($0 \le n \le 1$) argyrodites have been structurally characterized.

From the AC impedance measurements, the compositional dependencies of the ionic conductivity in the temperature interval from

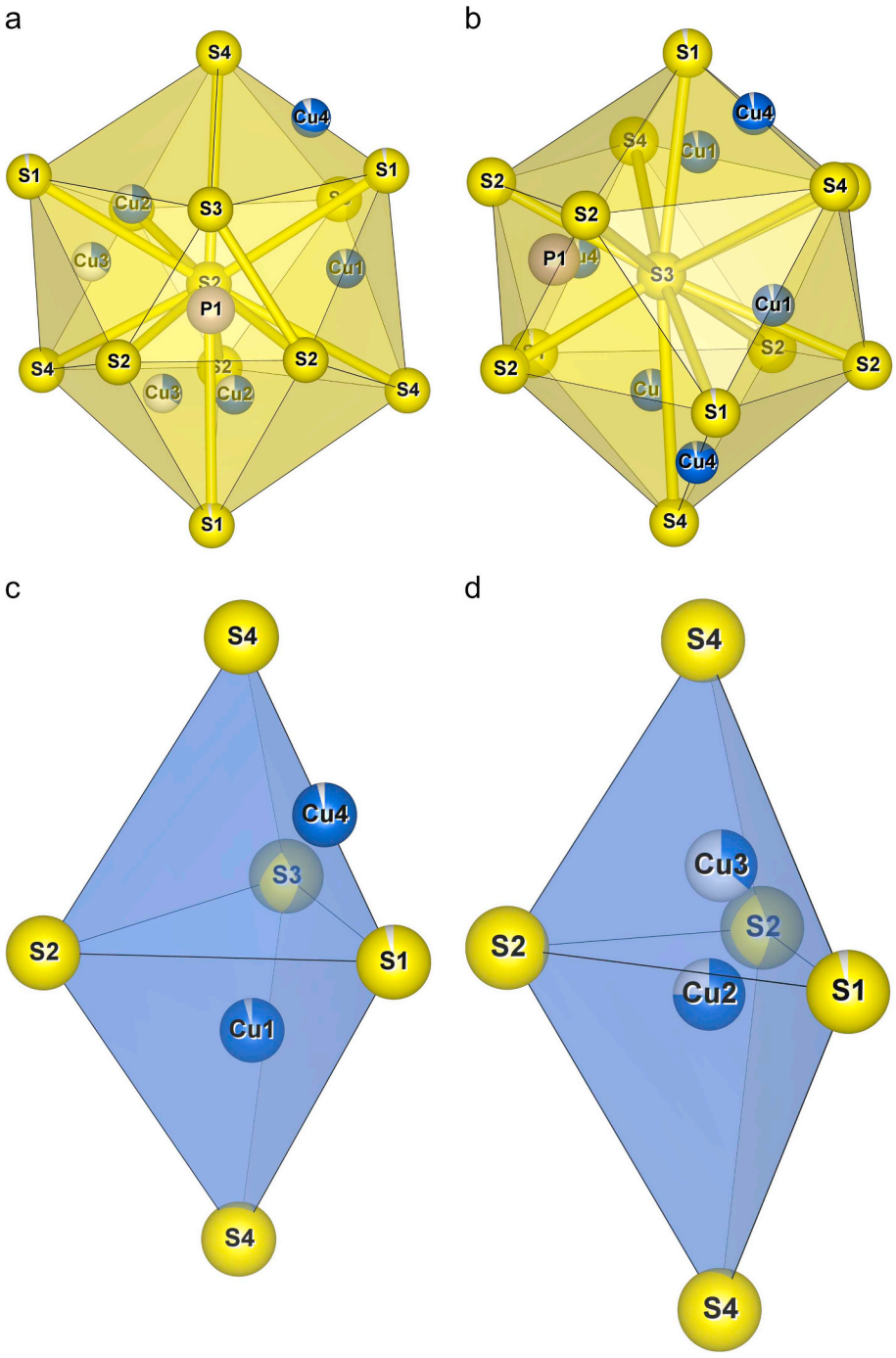

Fig. 7. Icosahedra [SS_{12}] centered by the atoms S2 (a) and S3 (b) and coordination of the copper atoms: Cu4, Cu1 (c), and Cu2, Cu3 (d) in the structure of Cu_7PS_6.

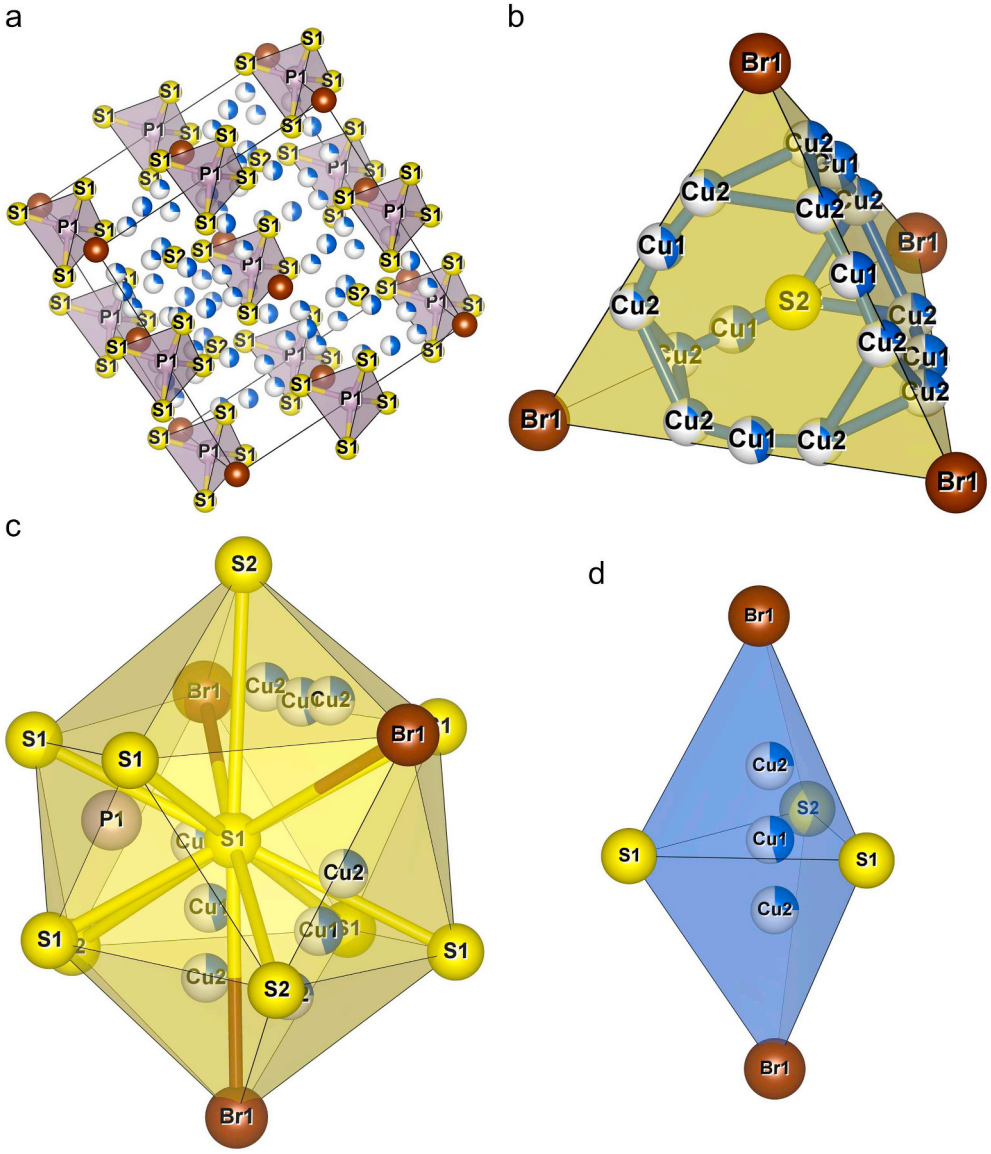

Fig. 8. Coordination tetrahedra [PS_4] (a) and [SBr_4] (b), icosahedron [SS_9Br_3] (c) and coordination of the copper atoms (d) in the structure of Cu_6PS_5Br.

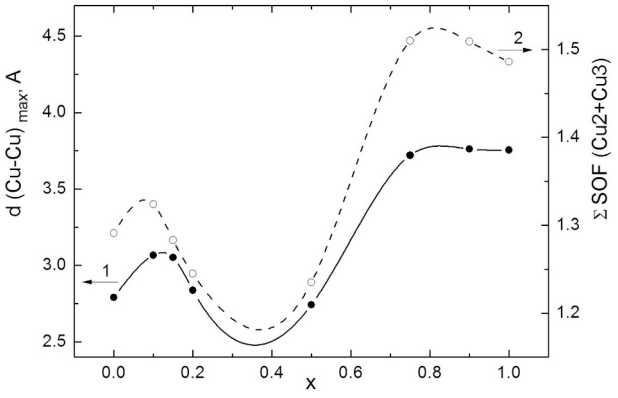

Fig. 9. Compositional dependencies of $d(Cu\text{-}Cu)_{max}$ (1) and ΣSOF (2) indicator for $Cu_{7-n}PS_{6-n}Br_n$ single crystals.

295 to 353 K as well as compositional dependence of the activation energy for the crystals in the Cu_7PS_6–Cu_6PS_5Br system have been determined. It is shown that the ionic conductivity in $Cu_{7-n}PS_{6-n}Br_n$ ($0 \le n \le 1$) argyrodites is defined by the migration of Cu2 and Cu3 atoms for Cu_7PS_6-based solid solutions and by the migration of Cu1 and Cu2 atoms for Cu_6PS_5Br-based solid solutions.

Two simple structural indicators have been proposed in order to predict the ionic conductivity of the copper argyrodites: (i) the sum of the SOF values of the positions for the migrating Cu atoms and (ii) the longest symmetrically independent distance between these atoms $d(Cu\text{-}Cu)_{max}$. The strong inverse correlation between $d(Cu\text{-}Cu)_{max}$ and ΣSOF values is revealed for $Cu_{7-n}PS_{6-n}Br_n$ ($0 \le n \le 1$) argyrodites.

References

[1] W.F. Kuhs, R. Nitsche, K. Scheunemann, The argyrodites - a new family of tetrahedrally close-packed structures, Mat. Res. Bull. 14 (1979) 241–248, https://doi.org/10.1016/0025-5408(79)90125-9.

[2] T. Nilges, A. Pfitzner, A structural differentiation of quaternary copper argyrodites: Structure – property relations of high temperature ion conductors, Z. Kristallogr. 220 (2005) 281–294, https://doi.org/10.1524/zkri.220.2.281.59142.

[3] I.P. Studenyak, V.O. Stefanovich, M. Kranjčec, D.I. Desnicac, Y.M. Azhnyuk, G.S. Kovacs, V.V. Panko, Raman scattering studies of Cu_6PS_5Hal (Hal = Cl, Br and I) fast-ion conductors, Solid State Ionics 95 (1997) 221–225, https://doi.org/10.1016/S0167-2738(96)00477-8.

[4] I.P. Studenyak, M. Kranjčec, G.S. Kovacs, V.V. Panko, Y.M. Azhniuk, D.I. Desnica, O.M. Borets, Y.V. Voroshilov, Fundamental optical absorption edge and exciton–phonon interaction in Cu_6PS_5Br superionic ferroelastic, Mater. Sci. Eng. B 52 (1998) 202–207, https://doi.org/10.1016/S0921-5107(97)00278-X.

[5] I.P. Studenyak, M. Kranjčec, G.S. Kovacs, V.V. Pan'ko, I.D. Desnica, A.G. Slivka, P.P. Guranich, The effect of temperature and pressure on the optical absorption edge in Cu_6PS_5X (X = Cl, Br, I) crystals, J. Phys. Chem. Solids 60 (1999) 1897–1904, https://doi.org/10.1016/S0022-3697(99)00220-6.
[6] A. Haznar, A. Pietraszko, I.P. Studenyak, X-ray study of the superionic phase transition in Cu_6PS_5Br, Solid State Ionics 119 (1999) 31–36, https://doi.org/10.1016/S0167-2738(98)00479-2.
[7] I.P. Studenyak, M. Kranjčec, G.S. Kovacs, V.V. Panko, V.V. Mitrovcij, O.A. Mikajlo, Structural disordering studies in $Cu_{6+\delta}PS_5I$ single crystals, Mater. Sci. Eng. B 97 (2003) 34–38, https://doi.org/10.1016/S0921-5107(02)00392-6.
[8] A. Gągor, A. Pietraszko, D. Kaynts, Diffusion paths formation for Cu^+ ions in superionic Cu_6PS_5I single crystals studied in terms of structural phase transition, J. Solid State Chem. 178 (2005) 3366–3375, https://doi.org/10.1016/j.jssc.2005.08.015.
[9] I.P. Studenyak, V.Y. Izai, A.I. Pogodin, O.P. Kokhan, V.I. Sidey, M.Y. Sabov, A. Kežionis, T. Šalkus, J. Banys, Structural and electrical properties of argyrodite-type Cu_7PS_6 crystals, Lith. J. Phys. 57 (2017) 243–251, https://doi.org/10.3952/physics.v57i4.3603.
[10] I.P. Studenyak, V.Y. Izai, V.I. Studenyak, S.O. Rybak, A.I. Pogodin, O.P. Kokhan, M. Kranjčec, Phase transitions and optical absorption edge in $(Cu_6PS_5Br)_{1-x}(Cu_7PS_6)_x$ mixed crystals, J. Alloys Compounds 735 (2018) 417–421, https://doi.org/10.1016/j.jallcom.2017.11.144.
[11] H.L. Bhat, Introduction to Crystal Growth: Principles and Practice, CRC Press, Boca Raton (FL) 2015.
[12] C. Yu, L. van Eijck, S. Ganapathy, M. Wagemaker, Synthesis, structure and electrochemical performance of the argyrodite Li_6PS_5Cl solid electrolyte for Li-ion solid state batteries, Electrochim. Acta 215 (2016) 93–99.
[13] J. Auvergniot, A. Cassel, D. Foix, V. Viallet, V. Seznec, R. Dedryvère, Redox activity of argyrodite Li_6PS_5Cl electrolyte in all-solid-state Li-ion battery: An XPS study, Solid State Ionics 300 (2017) 78–85.
[14] S. Wenzel, S.J. Seldmaier, C. Dietrich, W.G. Zeier, J. Janek, Interfacial reactivity and interphase growth of argyrodite solid electrolytes at lithium metal electrodes, Solid State Ionics 318 (2018) 102–112.
[15] S. Yubuchi, M. Uematsu, C. Hotehama, A. Sakuda, A. Hayashi, M. Tatsumisago, An argyrodite sulfide-based superionic conductor synthesized by a liquid-phase technique with tetrahydrofuran and ethanol, J. Mater. Chem. A 7 (2019) 558–566.
[16] A.I. Pogodin, A.P. Kokhan, I.E. Barchii, A.M. Solomon, Y. Stasyuk, Physicochemical interaction in the $CuBr$-Cu_2S-Cu_6PS_5Br quasi-ternary system, Russ. J. Inorg. Chem. 60 (2015) 741–745.
[17] H.M. Rietveld, A profile refinement method for nuclear and magnetic structures, J. Appl. Crystallogr. 2 (1969) 65–71, https://doi.org/10.1107/S0021889869006558.
[18] L.B. McCusker, R.B. Von Dreele, D.E. Cox, D. Louër, P. Scardi, Rietveld refinement guidelines, J. Appl. Crystallogr. 32 (1999) 36–50, https://doi.org/10.1107/S0021889898009856.
[19] A. Altomare, C. Cuocci, C. Giacovazzo, A. Moliterni, R. Rizzi, N. Corriero, A. Falcicchio, EXPO2013: a kit of tools for phasing crystal structures from powder data, J. Appl. Crystallogr. 46 (2013) 1231–1235, https://doi.org/10.1107/S0021889813013113.
[20] E. Jansen, W. Schäfer, G. Will, R values in analysis of powder diffraction data using Rietveld refinement, J. Appl. Crystallogr. 27 (1994) 492–496, https://doi.org/10.1107/S0021889893012348.
[21] V. Sidey, A. Shteyfan, Revised bond valence parameters for the P^{+5}/S^2 ion pair, J. Phys. Chem. Solids 103 (2017) 73–75, https://doi.org/10.1016/j.jpcs.2016.12.004.
[22] A.K. Ivanov-Schitz, I.V. Murin, Solid State Ionics, 1 Univ. Press, S.-Petersburg, 2000 (in Russian).
[23] I.P. Studenyak, M.M. Luchynets, V.Y. Izai, A.I. Pogodin, O.P. Kokhan, Y. Azhniuk, D.R.T. Zahn, Structural and optical properties of $(Cu_6PS_5Br)_{1-x}(Cu_7PS_6)_x$ mixed crystals, J. Alloys Compounds 782 (2019) 586–591, https://doi.org/10.1016/j.jallcom.2018.12.214.